frontiers | Frontiers in Materials

TYPE Original Research
PUBLISHED 02 May 2024
DOI 10.3389/fmats.2024.1388122

OPEN ACCESS

EDITED BY
João Reis,
Fluminense Federal University, Brazil

REVIEWED BY
Shengwen Tang,
Wuhan University, China
Jinyang Jiang,
Southeast University, China

*CORRESPONDENCE
Yanlin Huo,
hyl19950118@163.com
Dong Lu,
dong71.lu@connect.polyu.hk

RECEIVED 19 February 2024
ACCEPTED 15 April 2024
PUBLISHED 02 May 2024

CITATION
Huang J, Huo Y, Su Q, Lu D, Wu Y, Dong X and Gao Y (2024), Sustainable high-strength alkali-activated slag concrete is achieved by recycling emulsified waste cooking oil. *Front. Mater.* 11:1388122. doi: 10.3389/fmats.2024.1388122

Sustainable high-strength alkali-activated slag concrete is achieved by recycling emulsified waste cooking oil

Jinguang Huang[1,2], Yanlin Huo[3,4,5]*, Qunshan Su[1], Dong Lu[3,4,5]*, Yuanchao Wu[1], Xinhong Dong[1] and Yang Gao[1]

[1]Postdoctor Workstation, Henan D.R. Construction Group, Zhengzhou, China, [2]Research and Development Center, Henan Qingshui Construction Technology Co., Ltd., Xinxiang, China, [3]School of Civil Engineering, Harbin Institute of Technology, Harbin, China, [4]Key Lab of Structures Dynamic Behavior and Control of the Ministry of Education, Harbin Institute of Technology, Harbin, China, [5]Key Lab of Smart Prevention and Mitigation of Civil Engineering Disasters of the Ministry of Industry and Information Technology, Harbin Institute of Technology, Harbin, China

To mitigate the shrinkage of high-strength alkali-activated slag concrete (AASC), this paper introduces emulsified cooking oil (ECO) and emulsified waste cooking oil (EWCO) into the AASC system. The effects of admixing ECO and EWCO on the compressive strength, drying shrinkage, autogenous shrinkage, carbonation, and sulfuric acid resistance of the AASC are systematically explored. The optimization mechanism is also proposed based on the surface tension and microstructural analysis. The experimental results show that the admixing ECO and EWCO slightly reduce the compressive strength of the AASC by 7.8%. Interestingly, the admixing ECO and EWCO significantly reduce the drying shrinkage and autogenous shrinkage, simultaneously improving the resistance to carbonation and sulfuric acid of the AASC. Specifically, the introduction of 2 wt.% ECO and EWCO can reduce the autogenous shrinkage of the AASC by 66.7% and 41.0%, respectively. Microstructural observations reveal that the addition of ECO and EWCO can reduce the internal surface tension of the AASC, improve the transport and diffusion of the pore solution, and increase the absorbable free water of the slag, which in turn reduces the shrinkage of the composites. It also increases the ionic concentration in the pore solution, resulting in a more complete reaction of the AASC, which can optimize the pore structure and thus improve the durability of the AASC. This study proposes a promising way to develop sustainable alkali-activated slag concrete achieved by recycling waste materials.

KEYWORDS

alkali-activated slag concrete, emulsified cooking oil, emulsified waste cooking oil, recycling, durability, sustainable construction

1 Introduction

Rapid urbanization and dramatic population growth, among other factors, have raised the demand for new infrastructure and houses, and have further exacerbated the impact of the construction industry on the global environment (Juenger et al., 2011; Huo et al., 2022a; Yin et al., 2023; Lu et al., 2024a). The cement production process generates about 8% of total global emissions of carbon dioxide,

contributing significantly to the greenhouse effect and posing a significant threat to human health (Díaz et al., 2017; Huo et al., 2022b; Huo et al., 2023a). This is contrary to the current concept of green and sustainable development (Meyer, 2009; Lu et al., 2023a; Lu et al., 2024b). As such, the R&D of eco-friendly building materials to replace concrete has become one of the main focuses of scientific research (Huo et al., 2023b; Karikatti et al., 2023).

Alkali-activated slag concrete (AASC), a type of cement-free green cementitious material has emerged and developed in recent years (Huo et al., 2023c; Huo et al., 2023d). In particular, the main cementitious material, granulated blast furnace slag (GGBFS), is an industrial by-product produced during iron production, which has hydration potential and activity in alkaline environments (Thomas et al., 2018; Zheng et al., 2022; Lu et al., 2023b). AASC has significant environmental and economic benefits (Fu et al., 2023; Lu et al., 2024c). A Life Cycle Assessment reports that AASC has a Global Warming Potential (GWP) that is ~70% lower than PCC (Purnell, 2013; Huang et al., 2021). The application of AASC offers an extremely low carbon footprint, making it an ideal candidate for replacing cement in the development of concrete infrastructure (Amani et al., 2021; Huo et al., 2022a). However, the practical application of AASC has been very limited to date, mainly due to the AASC having high shrinkage (both autogenous shrinkage and drying shrinkage) and is prone to cracking at early ages, which seriously affects the safety of building structures (Bakharev et al., 2002; Sadeghian et al., 2022). Specifically, autogenous shrinkage and drying shrinkage can directly affect the long-term performance of concrete structures (Lu et al., 2023c), which can adversely affect the serviceability of concrete structures (Dai et al., 2022; Sadeghian et al., 2022). It is reported that the shrinkage of the AASC is 1.7–2 times higher than that of the PCC, mainly attributed to the fact that the Ca/Si ratio of C-(A)-S-H gel is lower than that in PCC and the absence of crystalline phases such as Portlandite (Bondar et al., 2018; Wang et al., 2020; Wang et al., 2021; Zhou et al., 2023; Geng et al., 2024). Additionally, the poor carbonation resistance of the AASC also limits its practical application (Weil et al., 2024).

Recently, some attempts have been adopted to inhibit shrinkage and improve the carbonation resistance of the AASC (Collins and Sanjayan, 2000; Huo et al., 2023e). For example, fiber, polypropylene glycol, and supplementary cementitious materials (SCM) have been incorporated into AASC to address these problems (Chi, 2012; Zhang et al., 2017). Additionally, lowering the alkali equivalent, increasing the silicate modulus, and increasing the curing temperature can help to reduce capillary pressure, thereby mitigating the drying shrinkage and improving the carbonation resistance of the AASC (Aydın and Baradan, 2021; Huo et al., 2024). However, the low efficiency, high energy consumption, and high cost of the above methods limit their practical applications (Zhao et al., 2020). One of the causes of concrete shrinkage is shrinkage stress, which is proportional to surface tension (Zhu et al., 2021). Some researchers have found that reducing the surface tension of pore solutions in concrete can significantly reduce shrinkage (Ou et al., 2022). Cooking oil and waste cooking oil are less dense than pure water and emulsifying them significantly reduces the surface tension. At least 10 million tons of used cooking oil are produced in China every year, but the current utilization rate is less than 10%. The addition of waste oil into the AASC system can alleviate the environmental pressure and has great potential to reduce shrinkage and improve carbonization and other durability properties.

In this study, edible oil and waste cooking oil are first emulsified and then emulsified cooking oil (ECO) and emulsified waste cooking oil (EWCO) are introduced into the AASC system to improve the durability of the AASC. The effects of admixing ECO and EWCO on compressive strength, drying shrinkage, autogenous shrinkage, carbonation depth, and sulfuric acid resistance of the AASC are investigated. The mechanism of admixing ECO and EWCO in the AASC system is further explored by microstructure and pore structure analysis. This study may not only provide new ideas for the shrinkage reduction of AASC but also rationalize the use of waste cooking oil and reduce environmental pollution. Further, for higher strength ultra-high performance concrete (UHPC), waste cooking oil is also expected to reduce its shrinkage and improve its durability.

2 Experimental program

2.1 Materials

The GGBFS is purchased from Shijiazhuang, Hebei Province. Its main physical parameters are exhibited in Table 1 and compared with the standard of S95 grade slag following GB/T18046-2017. The chemical composition of the GGBFS was acquired using X-ray fluorescence spectroscopy (Table 2). Furthermore, the chemical compositions of the GGBFS were also characterized using the activity coefficient, alkalinity coefficient, water hardness coefficient, and quality coefficient, and the results indicated that all the above indicators meet the requirements. Figure 1 shows the particle size distribution of the GGBFS.

The activator was a $Na_2O{\cdot}SiO_2$ solution, commonly referred to as water glass. Its modulus (Ms) is 3.48. $\omega(SiO_2)$ = 25.6%, $\omega(Na_2O)$ = 7.6%. NaOH (99.9 wt%) was used to adjust the modulus of the water glass.

The natural coarse and fine aggregates used were both from Harbin. The parameters of natural coarse and fine aggregate (natural river sand) are listed in Table 3. The natural sand has a fineness modulus of 2.87. The chemical compositions of the natural fine aggregate were characterized by XRF, as shown in Table 4.

The cooking oil (CO) and waste cooking oil (WCO) were obtained from the school cafeteria of Harbin Institute of Technology, China. The emulsifiers were Span-80 and OP-10 emulsifiers. The properties of the oils and emulsifiers are summarized in Table 5.

2.2 Mixture design and preparation of concrete

2.2.1 Emulsification of CO and WCO

The CO/WCO needs to be emulsified before preparing the concrete, which is done as follows: 1) Pour the CO/WCO into a conical flask, heat it to 60°C with a thermostatic water bath and stir it at 1,200 rpm for 30 min; 2) Prepare water of 1.5 times the mass of CO/WCO. Add 2/3 of water and 7.5 wt.% of complex emulsifier (90% Span-80% and 10% OP-10) in the conical flask and continue mixing for 20 min at the same mixing speed; 3) Finally, pour the

TABLE 1 Physical properties of GGBFS.

Physical parameter		GGBFS	S95 standard indicators
Density (g/cm^3)		2.94	≥2.80
Specific surface area (m^2/kg)		410	≥400
L.O.I (%)		0.76	≤1.0
Moisture content (%)		0.01	≤1.0
Activity index (%)	7 days	90	≥70
	28 days	98	≥95

TABLE 2 Chemical compositions of GGBFS (wt.%).

	CaO	SiO_2	Al_2O_3	MgO	SO_3	TiO_2	Na_2O	Fe_2O_3
GGBFS	40.95	30.74	14.87	8.95	1.83	1.53	0.37	0.52

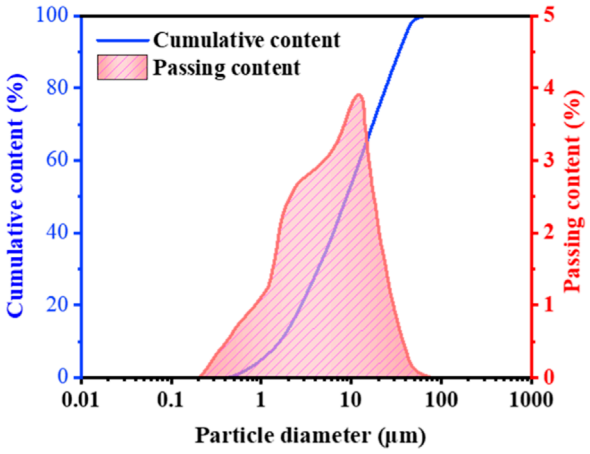

Particle (μm)	Content (%)
0.100	0.00
0.300	0.00
0.500	0.53
1.000	4.94
2.000	13.40
5.000	33.73
10.000	53.35
45.000	97.30
75.000	99.96
100.000	100.00

FIGURE 1
Particle size distribution of GGBFS.

TABLE 3 Properties of aggregates.

	Density (g/cm^3)	Modulus fineness	Crushing index (%)	Water absorption (%)
Fine	2.88	2.87	9.0	1.40
Coarse	2.86	—	2.09	1.21

TABLE 4 Chemical composition of fine aggregate (wt.%).

Chemical composition	CaO	SiO_2	Al_2O_3	K_2O	Na_2O	Fe_2O_3	MgO
Fine aggregate	1.39	75.59	13.18	4.42	3.28	1.46	0.11

TABLE 5 Properties of oils and emulsifiers.

	Colour	Condition	Density (g/cm^3)	Main component
OP-10	Yellow	Liquid	0.98	$C_{35}H_{64}O_{11}$
Span-80	Transparent	Liquid	0.92	$C_{24}H_{44}O_6$
Cooking oil	Yellow	Liquid	0.88	Fatty acid
WCO	Black brown	Liquid	0.65	Fatty acid

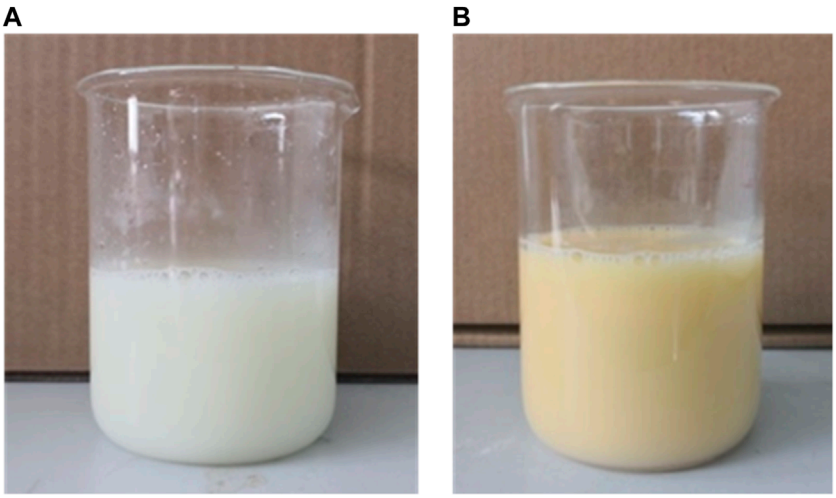

FIGURE 2
(A) Emulsified cooking oil and **(B)** emulsified waste cooking oil.

remaining water into the solution at the same stirring speed and stir for a further 20 min. Figure 2 shows the ECO and EWCO.

2.2.2 Preparation of concrete

Two different strength grades of concrete were selected in this study: normal strength and higher strength of concrete with a water-binder (w/b) ratio of 0.5 and 0.35 and binder-to-sand ratio of 0.45 and 0.82, respectively. The Na ion concentration of the base activator was immobilized at 3 wt% of GGBFS. The dosages of the ECO and EWCO were 1 and 2% by the weight of the GGBFS, respectively.

At first, the coarse and fine aggregates were oven-dried. Then, the solid components were blended for 2 min. The mixed alkali solution and ECO/EWCO were inserted into the mixer and mixing continued for 2 min. After that, the fresh concrete was cast into the moulds and cured at standard conditions. The ratio of the mixtures is summarized in Table 6.

2.3 Test methods

2.3.1 Compressive strength

The cubic compressive strength (100 mm × 100 mm × 100 mm) was determined according to the standard GB/T 50010-2010. The loading rate of the test was 2.4 kN/s. The age of the compressive strength was tested at 7 days and 28 days, respectively. All final results reported are the average of three replicate tests.

2.3.2 Drying shrinkage

The dry shrinkage was tested by digital extensible measuring equipment following GB/T 50082-2009. The size of the specimen was 100 mm × 100 mm × 515 mm. Long-term strain measurements were performed on both concrete surfaces vertically to the caste plane within the test period.

2.3.3 Autogenous shrinkage

The autogenous shrinkage test was performed using 100 mm × 100 mm × 515 mm specimens. An eddy current displacement sensor (ECDS) was used to measure the autogenous shrinkage. The blend was poured into a steel mold immediately following stirring, and a stainless target seat was inset into the specimen, which was deformed at the same time as the AASCs. The method used to measure autogenous shrinkage is demonstrated in Figure 3.

2.3.4 Carbonation

The carbonation of concrete was assessed according to GB/T 50082-2009. The specimens were placed in a carbonation chamber at 20°C ± 2°C and 70% ± 5% relative humidity. Concrete fracture surfaces were sprayed with 1% alcoholic phenolphthalein solution and the neutralization depth was monitored.

10.3389/fmats.2024.1388122

TABLE 6 Mixing proportion of AASC (kg/m^3).

Strength level	Name	GGBFS	Water	Coarse aggregate	Fine aggregate	Water glass	NaOH	Additive
Normal Strength	Control-0.5	360	143.56	1197.42	798.28	52.06	13.02	0
	ECO-1%-0.5	360	143.56	1197.42	798.28	52.06	13.02	7.2
	EWCO-1%-0.5	360	143.56	1197.42	798.28	52.06	13.02	7.2
	ECO-2%-0.5	360	143.56	1197.42	798.28	52.06	13.02	14.4
	EWCO-2%-0.5	360	143.56	1197.42	798.28	52.06	13.02	14.4
High Strength	Control-0.35	571.4	136.8	1042.1	694.7	87.3	21.2	0
	ECO-1%-0.35	571.4	128.7	1042.1	694.7	87.3	21.2	14.2
	EWCO-1%-0.35	571.4	128.7	1042.1	694.7	87.3	21.2	14.2
	ECO-2%-0.35	571.4	120.5	1042.1	694.7	87.3	21.2	28.5
	EWCO-2%-0.35	571.4	120.5	1042.1	694.7	87.3	21.2	28.5

2.3.5 Sulphuric acid resistance

It was evaluated for sulfuric acid resistance according to ASTM C267. Cubic samples of 100 mm × 100 mm × 100 mm were immersed in a 3% solution of sulfuric acid after 7 days of curing. After 7, 14, 28, 60, 90, 120, and 180 days of immersion, the resistance was evaluated based on the weight loss as described in Eq. 1.

$$\Delta W_n = \frac{M_0 - M_n}{M_0} \times 100 \quad (1)$$

where $\triangle W_n$ is the mass loss rate (%), M_0 is the initial mass of the samples (g), and M_n is the mass of the samples after n days of soaking in sulfuric acid solution.

2.4 Microscopic investigations

2.4.1 Surface tension

The liquid surface tension of the composites was performed using a BZY-type surface tension instrument. Before testing, the instrument needs to be preheated for 30 min. After preheating, the platform is cleaned with flowing water and then the sample of the measured solution is placed in the sample platform. Controlling the knob makes the liquid level of the sample in contact with the induction device of the tester, and the reading is taken after the constant.

2.4.2 Mercury intrusion porosimeter (MIP)

The pore size distribution of the concrete was tested on typical samples using an IV 9510 Mercury Intrusion Porosimeter (MIP), which has an intrusion pressure range of 0–60,000 psi and is capable of measuring pore sizes up to 3.0 nm in diameter.

2.4.3 Backscattered electron (BSE) and energy dispersive spectroscopy (EDS)

Samples were cut into 3–5 mm pieces for BSE and EDS testing. The dried samples were dipped into epoxy resin and buffed to a 0.25 μm surface fineness with diamond paste. The sample surface was applied with carbon and then dried in a low vacuum desiccator prior to analysis.

3 Results and discussion

3.1 Compressive strength

As shown in Figure 4, the 7-day compressive strength of all mixtures achieved over 70% of its corresponding 28-day strength. It is more pronounced in the high-strength concrete group, where the 7-day strengths of all the composites are close to about 85% of their corresponding 28-day strengths. However, adding ECO and EWCO harmed the compressive strength of the AASC, but the effect was minimal. As the w/b ratio is 0.5 in AASC, the effects of admixing ECO and EWCO on the 28-day strength of the AASC were small in magnitude, and the lowest strength was obtained with 2% EWCO, which is only reduced by 7.8%, mainly due to admixing ECO has a delaying effect on the setting time of the AASC, simultaneously, it can help to improve the internal pore structure of the concrete and reduce

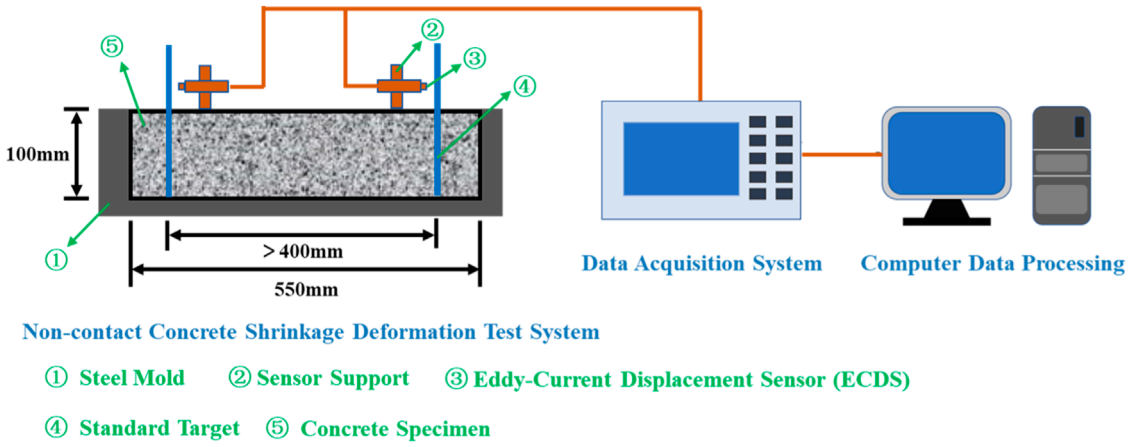

FIGURE 3
Autogenous shrinkage test method for AASC.

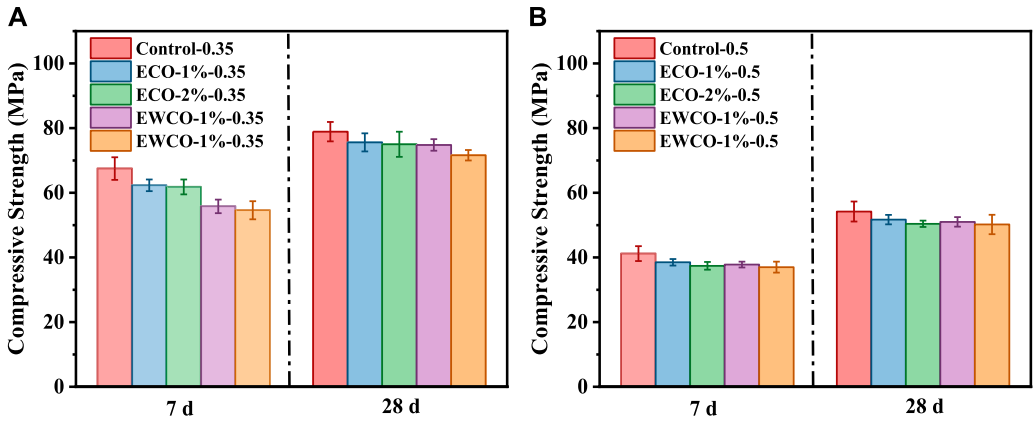

FIGURE 4
Compressive strength of AASC of different w/b ratios with ECO and EWCO: **(A)** w/b = 0.35, and **(B)** w/b = 0.5.

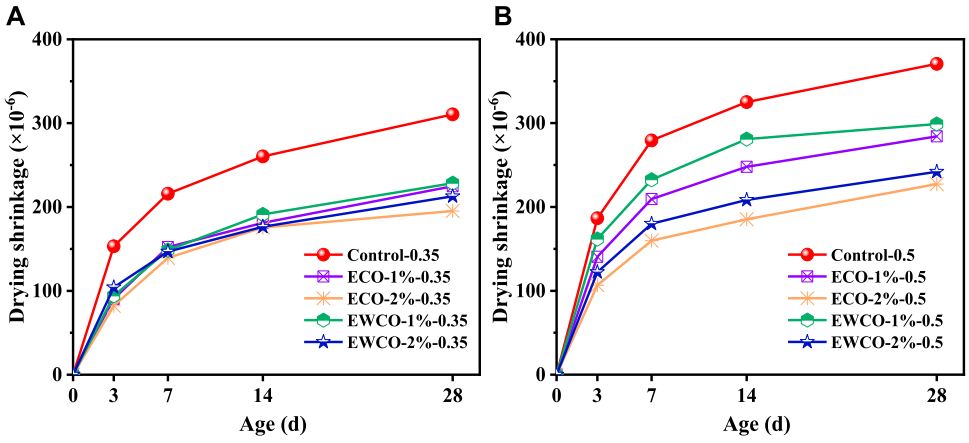

FIGURE 5
Drying shrinkage of AASCs of different w/b ratios with ECO and EWCO: **(A)** w/b = 0.35, and **(B)** w/b = 0.5.

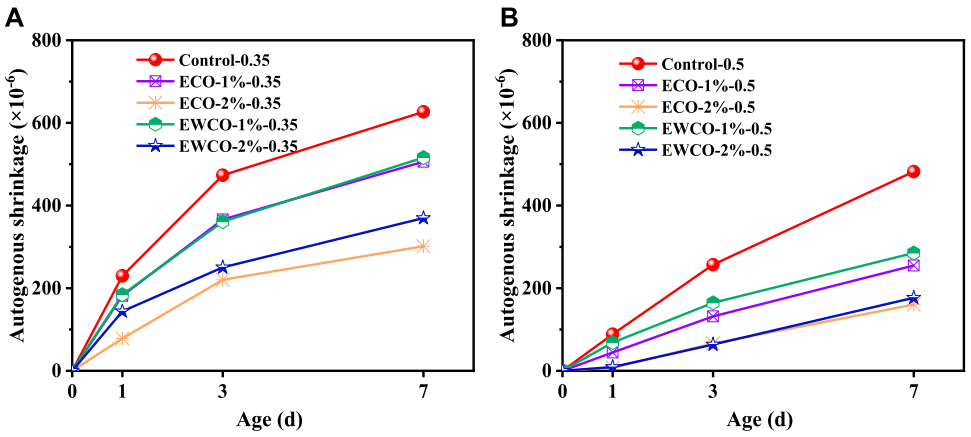

FIGURE 6
Autogenous shrinkage of AASCs of different w/b ratios with ECO and EWCO: **(A)** w/b = 0.35, and **(B)** w/b = 0.5.

the number of harmful pores (Huo et al., 2023f). Additionally, the addition of ECO can reduce the microcracks of the AASC, so the positive effect partially offsets the negative effect of delayed setting time.

In high-strength AASC, the effect of adding 1% ECO on the strength was still small, and when the dosage of additive increased to 2%, the strength of the EWCO-modified concrete attained the lowest value, about 15% lower (Figure 4B), mainly because the impurities contained in EWCO lead to a greater negative effect in the denser hydrated structure relative to the normal hydrogel ratio, affecting the denseness of the structure. Compared to ECO, the unsaturated fatty acid content contained in EWCO is lower, and negatively affects the pore structure of concrete, therefore, the negative impact of using EWCO on the strength of concrete is greater compared to that of employing ECO.

In general, the addition of ECO had minimal effect on the strength of the AASC, and the addition of EWCO caused some negative effects on the strength of the AASC, but is recycling EWCO in concrete production is still a feasible approach considering the added value of resourceful reuse of EWCO.

3.2 Drying shrinkage

As suggested in Figure 5, the addition of either ECO or EWCO can significantly reduce the drying shrinkage of the concrete. In which, the effect of shrinkage reduction by using ECO was slightly better than that of employing EWCO in both strength grades of AASC. The addition of ECO can reduce the drying shrinkage of alkali-slag concrete by about 30%, mainly attributed to the fact that the addition of ECO can effectively reduce the surface tension of the materials in the AASC and thus the capillary pressure (will be illustrated in the following section), resulting in a reduction in a lowered shrinkage of the concrete. Also, the improved pore structure was another reason for the reduction in drying shrinkage, as the internal porosity of the concrete was reduced the channels for internal and external moisture exchange were blocked, and thus the drying shrinkage of alkali-slag concrete was reduced significantly (Liao et al., 2023a; Liao et al., 2023b).

It was also found that the drying shrinkage reduction decreased with increasing the dosage of ECO and EWCO (Figure 5B). Especially, when the w/b ratio is 0.35, the drying shrinkage of concrete with 2% ECO or EWCO was only about 10% lower than that of the concrete incorporating 1% ECO or EWCO. The reason is that the structure of AASC is already dense enough, and the degree of internal and external water exchange is not high, and increasing the dosage of ECO and EWCO cannot further greatly improve the ability to hinder the internal and external water exchange of the AASC. Therefore, the overdosage of ECO and EWCO does not significantly reduce the drying shrinkage of the AASC.

3.3 Autogenous shrinkage

In Figure 6, compared with drying shrinkage, autogenous shrinkage of AASC is dramatically higher. On the 1st day, the autogenous shrinkage of all mixtures grows slowly. It is believed that the specimen may also expand at an early stage due to the hydration of the binder.

The autogenous shrinkage of the AASC with w/b ratios of 0.5 and 0.35 was 481 and 627 μm/m, respectively, after 7 days of curing. The addition of 1% ECO can reduce the autogenous shrinkage of concrete to 255 and 506 μm/m, respectively. And the addition of 1% EWCO can reduce the autogenous shrinkage of concrete by 40.8% and 17.6%, respectively. As the dosage of ECO and EWCO increased to 2%, the reduction is significantly higher, especially, since the addition of 2% ECO in low-strength concrete and high-strength concrete can reduce the autogenous shrinkage by about 66.7% and 51.9%. With increasing the dosage of ECO and EWCO, the internal surface tension of the AASC decreased accordingly, which reduced the capillary pressure in the AASC, thus further reducing shrinkage.

The shrinkage reduction effect of EWCO was slightly lower than that of ECO. This may be due to impurities contained in

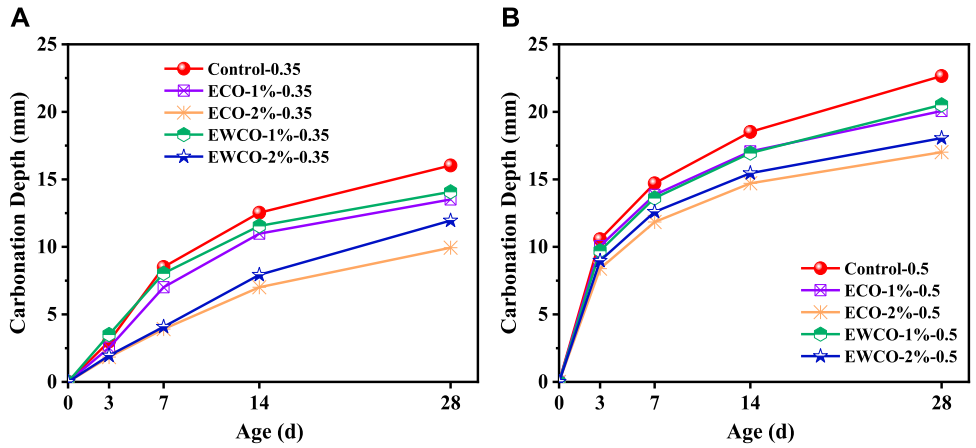

FIGURE 7
Carbonation depth of AASCs of different w/b ratios with ECO and EWCO: **(A)** w/b = 0.35, and **(B)** w/b = 0.5.

EWCO that may cause the binder to lose fluidity and inhibit the reaction between the oil and the binder. At all ages, the autogenous shrinkage of the AASC containing EWCO is approximately greater than that of the concrete incorporating ECO by less than 10% for the same substitution rate, which is considered to be within the acceptable range.

Overall, the use of 2% ECO and EWCO can reduce the autogenous shrinkage of the AASC by about 50%–60% and reduce the drying shrinkage value by about 30%. As such the use of ECO and EWCO can effectively limit the shrinkage of AASC, which has great potential in practical applications.

3.4 Carbonation depth

In Figure 7, the carbonation depth of AASC decreases as the w/b ratio decreases. At a low w/b ratio, the structure of AASC was denser, and the channels for external CO_2 to invade the interior of AASC were blocked. The carbonation depth of AASC increased rapidly in the first 7 days and then gradually stabilized. The ECO can effectively reduce the carbonation, mainly due to the addition of ECO can optimize the pore structure of AASC, thus effectively blocking the pathway of carbon dioxide. The effect of ECO was slightly better than that of EWCO, which was attributed to its higher active ingredient than EWCO, while the impurities in EWCO would harm the internal densification of AASC. The addition of 2% EWCO can reduce the 28-day carbonation depth of the AASC by 20% in each group. Effectively reducing the carbonation rate of AASC plays a protective role for steel reinforcement in reinforced concrete structures.

The addition of 2% ECO can reduce the carbonation depth of concrete by 37.5% in the 0.35 w/b ratio group. The addition of EWCO resulted in a carbonation depth of only about 10 mm. Considering the necessity of high-rise and long-life buildings in the future, the addition of ECO and EWCO to a low water-to-binder ratio AASC can further improve the carbonation resistance of high-performance concrete and promote its practical applications.

3.5 Sulphuric acid resistance

Figure 8 shows the effects of different w/b ratios and different dosages of ECO and EWCO on the weight loss of AASC when immersed in a 3% sulfuric acid solution for 180 days. During the first 28 days, all specimens showed a slight increase in weight. No significant damage was observed on the surface or edges of any of the specimens. Compared to the specimens with ECO and EWCO, the control specimens exhibited a greater weight increase due to higher water absorption. This is consistent with the carbonization results that ECO and EWCO improved the pore structure of AASC.

The resistance of AASCs with ECO and EWCO was slightly higher than the control concrete, mainly due to denser structure and lower porosity caused by ECO and EWCO. The application of ECO and EWCO may fill the pores in the AASC matrix and restrain the reaction between sulphuric acid and binder. The weight variations of specimens decreased with increasing the dosage of ECO and EWCO. The effect of EWCO on the improvement of acid resistance was slightly lower than ECO, mainly due to the higher porosity caused by the impurities in EWCO. The addition of ECO and EWCO can further improve the sulphuric acid resistance of the AASC.

3.6 Surface tension

As shown in Figure 9, the surface tension of water at room temperature was 72.3 mN/m. When ECO and EWCO were added, the surface tension of the liquid decreased substantially. The surface tension of the liquid was 36.5 mN/m and 36.3 mN/m when the concrete contained 1% and 4% ECO, respectively. The addition of EWCO was similar to that of ECO, and its liquid surface tension was about 3% lower than that of ECO at the same dosage because the density of EWCO was lower than that of ECO. When the dosage of ECO and EWCO was raised, the surface tension varied little with the increase in substitution rate of ECO and EWCO.

The strong cohesion between water molecules in the material pore solution made the surface tension of water higher. When ECO and EWCO were added, the water molecules in the pore solution

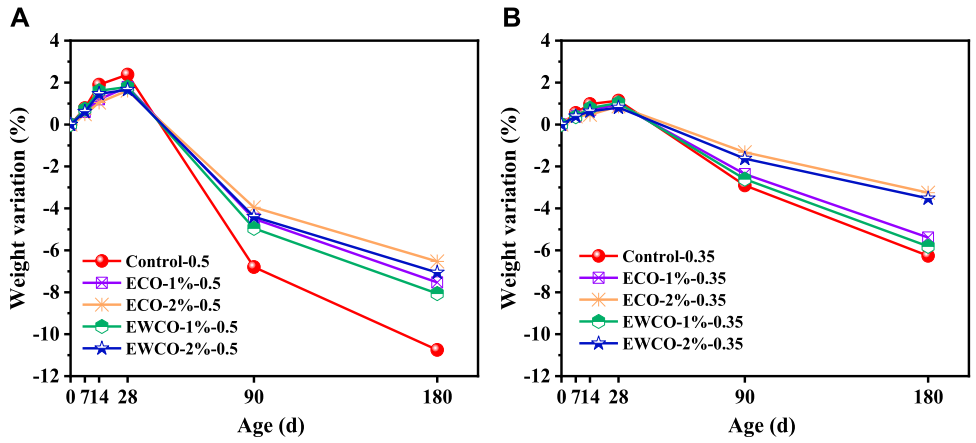

FIGURE 8
Sulphuric acid resistance of AASCs of different w/b ratios with ECO and EWCO: **(A)** w/b = 0.35, and **(B)** w/b = 0.5.

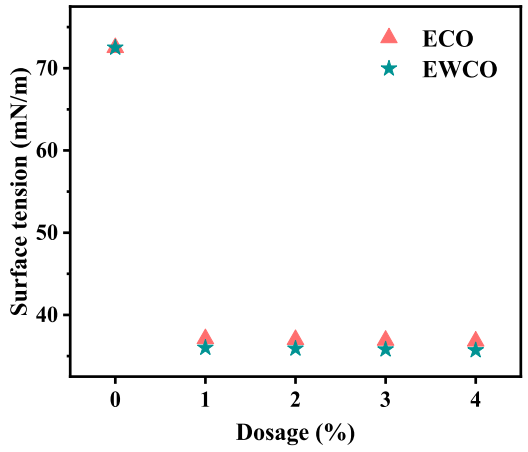

FIGURE 9
Surface tension of solution with various dosages of ECO and EWCO.

would be activated by the surface activation of ECO and EWCO. The force between ECO and EWCO and a water molecule was much smaller than the force between two water molecules, which changed the distribution and arrangement of water molecules on the surface of the pore solution, and therefore significantly lowered the surface tension of the pore solution. The surface tension of the pore solution is usually directly related to its transport and diffusion in the pore diameter, and a lower surface tension of the pore solution represents a stronger transport and diffusion ability. Therefore, as suggested in Figure 10, after the incorporation of ECO and EWCO, more water inside the material is adsorbed by the physical phase of the slag due to the higher transport and diffusion properties of the pore solution, and the resulting water consumption due to internal hydration (autogenous shrinkage), as well as water exchange due to the difference between the internal and external humidity (drying shrinkage) is significantly reduced, which leads to the lower autogenous and drying shrinkage results of the material.

3.7 MIP analysis

In normal-strength AASC, specimens with ECO added had slightly higher pore volumes than control samples in the pore size interval from 200 to 500 nm (Figure 11). However, the difference in pore distribution between the groups was minimal at pore diameters greater than 40 nm or less than 11 nm. Differences in pore size existed mainly between pores with diameters between 11 and 27 nm. When the pore diameter was less than 40 nm, a peak pore size point was present in all groups. The addition of ECO drastically reduced the pores between 14 and 40 nm. In particular, the number of pores between 17 and 27 nm was reduced by approximately 90% with the addition of ECO in concrete.

The effects of ECO and EWCO on the pore structure in high-strength AASC are similar to those of normal-strength AASC, the admixing ECO and EWCO mainly affected the porosity in the mesopore pore size range, with an overall shift of the curve towards smaller pores. Similarly, a peak pore size point existed in all groups. The peak pore size of the control group was around 15 nm, while the peak pore sizes of AASC with 2% ECO and EWCO were 9 nm and 11 nm, respectively.

The specific results of the mercury pressing experiments are given in Table 7. The admixing ECO or EWCO can significantly reduce the median pore size, average pore size, and porosity of AASC in both normal-strength and high-strength AASC. Especially, the addition of 2% ECO or EWCO can reduce the concrete by 19.7% and 21.8%, respectively. The reduction of overall harmful pores was very favourable to the development of AASC's durability. This is mainly dependent on the saponification reaction generated by the addition of ECO and EWCO to AASC, in which the lipids in the oil and the bases in AASC react with each other to fill some of the pores and optimize the pore structure.

3.8 BSE-EDS

Figure 12 shows the BSE images of the control group and the high-strength AASC with 2% EWCO. The microcracks of the

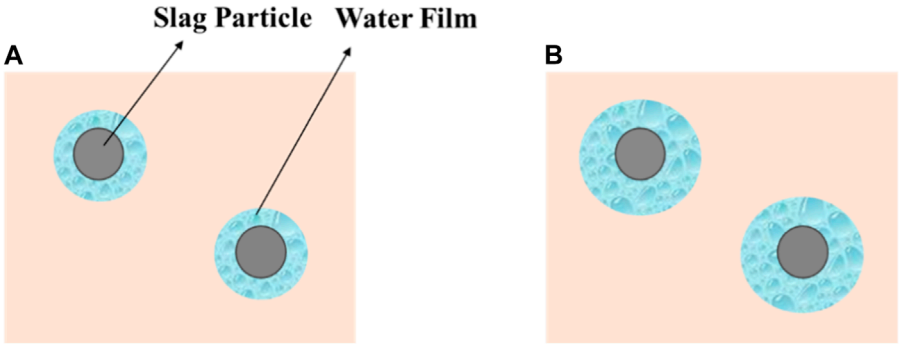

FIGURE 10
The mechanism of reduction effect of EO or EWCO: **(A)** Control, **(B)** EO or EWCO.

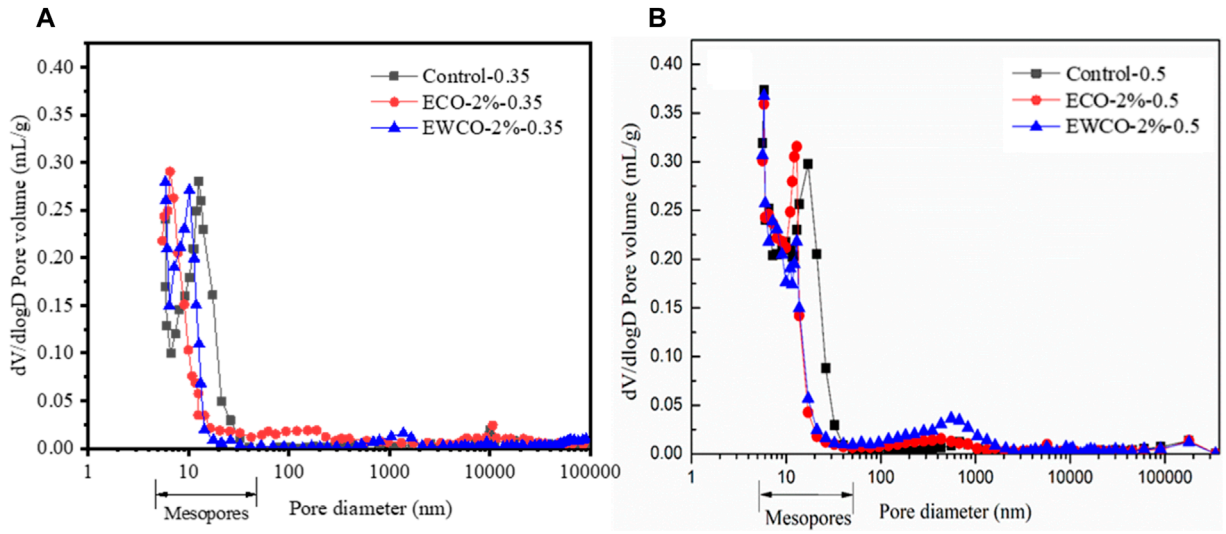

FIGURE 11
dV/dlog D pore size distribution curves of AASCs with 2% ECO and EWCO: **(A)** w/b = 0.35, **(B)** w/b = 0.5.

TABLE 7 Results of MIP test.

W/B	Control		ECO-2%		EWCO-2%	
	0.35	0.5	0.35	0.5	0.35	0.5
Median pore diameter (Volume, nm)	10.10	14.50	6.50	11.30	7.30	12.30
Average pore diameter (4V/A, nm)	10.30	12.70	8.20	11.40	8.40	12.70
Porosity (%)	18.88	27.99	17.08	21.90	17.13	22.48

specimens with EWCO were less than control group, which suggests that EWCO has the property of reducing AASC cracking. The C, O, and Ca elements of the specimens were further analyzed, and considering the chemical composition of the mineral powder and edible oil, it was concluded that the EWCO was saponified with the AASC to produce calcium fatty acids. Calcium advanced fatty acids are often used as surfactants in the industry to reduce the gravitational force between surface molecules, and the addition of such substances to AASC reduces the liquid flow in the pores of the concrete, which reduces the shrinkage stress, and consequently the shrinkage of the concrete.

Combined with the mechanism analysis of surface tension and MIP in the previous section, as well as the results of compressive strength, shrinkage, carbonation, and sulfuric acid

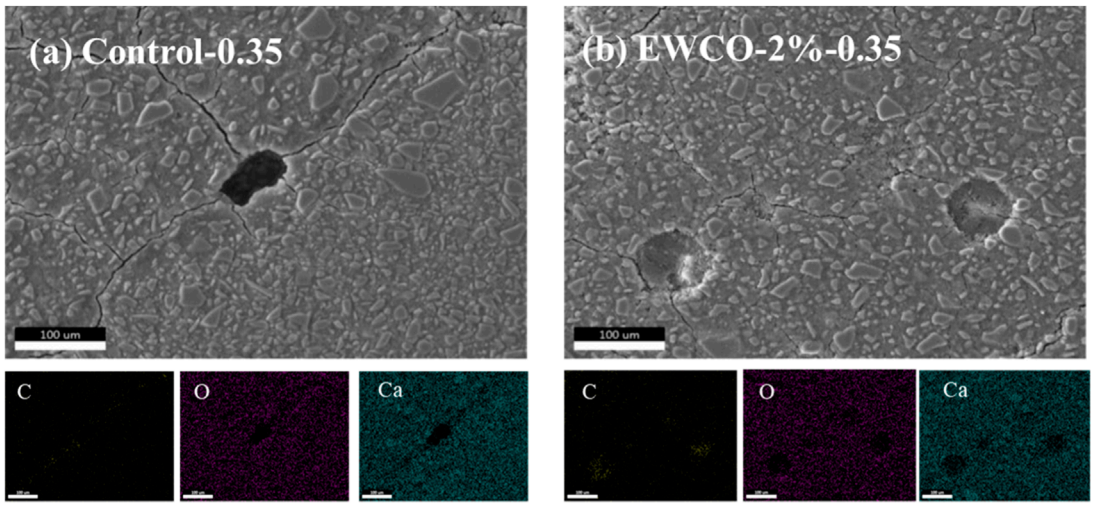

FIGURE 12
BSE images and EDS analysis of AASCs with various dosages of ECO and EWCO: **(A)** Control-0.35, and **(B)** EWCO-2%-0.35.

erosion resistance, the effects brought by ECO and EWCO are analysed comprehensively. 1) The inclusion of ECO and EWCO led to a reduction in the internal surface tension of AASC, which improved the transport and diffusion capacity of the pore solution, increasing the free water that could be adsorbed in the matter phase on the surface of the mineral powders, and a reduction in the exchange of water caused by the humidity difference in the concrete, which in turn reduced the shrinkage. 2) The free water adsorbed in the physical phase will hinder the contact between the mineral powder and the alkali exciter at an early stage, reducing the early strength of the concrete. 3) Also triggered by the reduction of surface tension, the stronger dissolution drive and the physical scouring effect of the stronger pore solution flow increased the ion concentration in the pore solution in the long-term perspective. AASC mixed with ECO and EWCO had a more complete degree of reaction of the mineral powders during the hydration and precipitation stage, which reduced the porosity and therefore compensated for the coagulation hindering effect caused by the early adsorption of water (Tang et al., 2021). Therefore, the incorporation of ECO and EWCO did not have a significant negative effect on the long-term strength. Instead, the reduced porosity resulted in a less permeable AASC structure, which improved the resistance to carbonation and sulfuric acid attack.

4 Conclusion

This study investigated the effect of emulsified cooking oil (ECO) and emulsified waste cooking oil (EWCO) on the properties of alkali-activated slag concrete (AASC) systems. In particular, the compressive strength, drying shrinkage, autogenous shrinkage, carbonation, and sulfuric acid resistance of AACS were systematically investigated to explore its potential for practical applications. The main findings of this study are as follows:

(1) The addition of ECO or EWCO had a minor negative effect on the compressive strength of the AASC. The compressive strength of the AASC decreased further with increasing the dosage of additives, but the maximum reduction for compressive strength is only 7.8%. The lower content of unsaturated fatty acids in EWCO had a significant negative impact on compressive strength compared to using ECO in the AASC system.
(2) The admixing ECO and EWCO can significantly reduce the drying shrinkage of the AASC, especially at high-strength composites. The shrinkage reduction effect of the EWCO is slightly lower than that of ECO, and its improvement is only 10% less than that of ECO. The drying shrinkage of the AASC was also reduced when the ECO or EWCO dosage was increased from 1% to 2%.
(3) The admixing ECO and EWCO can both effectively improve the carbonation and sulfuric acid resistance of the AASC. With the increase in the dosage of ECO and EWCO, the effect of carbonation and sulfuric acid resistance of the AASC performed better.
(4) The surface tension, MIP, and BSE-EDS analyses all showed that the addition of ECO and EWCO lowered the internal surface tension of the AASC, improved the transport and diffusion of the pore solution, and increased the absorbable free water of the slag, which in turn reduced the shrinkage. It also increased the ionic concentration in the pore solution, leading to a more complete reaction of the AASC, which optimized the pore structure and improved the durability of the AASC.

Data availability statement

The original contributions presented in the study are included in the article/supplementary material, further inquiries can be directed to the corresponding authors.

Author contributions

JH: Data curation, Formal Analysis, Investigation, Writing–original draft. YH: Conceptualization, Data curation, Investigation, Methodology, Project administration, Supervision, Validation, Visualization, Writing–review and editing. QS: Funding acquisition, Validation, Writing–review and editing. DL: Conceptualization, Investigation, Methodology, Software, Validation, Visualization, Writing–review and editing. YW: Supervision, Writing–review and editing. XD: Funding acquisition, Supervision, Writing–review and editing. YG: Software, Writing–review and editing.

Funding

The authors declare that financial support was received for the research, authorship, and/or publication of this article. The National Key R&D Program Project (No. 2022YFC3801405-04) for current research are gratefully acknowledged.

Conflict of interest

Authors JH, QS, YW, XD, and YG were employed by Henan D. R. Construction Group. Author JH was employed by Henan Qingshui Construction Technology Co., Ltd.

The remaining authors declare that the research was conducted in the absence of any commercial or financial relationships that could be construed as a potential conflict of interest.

Publisher's note

All claims expressed in this article are solely those of the authors and do not necessarily represent those of their affiliated organizations, or those of the publisher, the editors and the reviewers. Any product that may be evaluated in this article, or claim that may be made by its manufacturer, is not guaranteed or endorsed by the publisher.

References

Amani, A., Ramezanianpour, A. M., and Palassi, M. (2021). Investigation on the sustainable use of electric arc furnace slag aggregates in eco-friendly alkali-activated low fineness slag concrete as a green construction composite. *J. Clean. Prod.* 307, 127257. doi:10.1016/j.jclepro.2021.127257

Aydın, S., and Baradan, B. (2021). Sulfate resistance of alkali-activated slag and Portland cement based reactive powder concrete. *J. Build. Eng.* 43, 103205. doi:10.1016/j.jobe.2021.103205

Bakharev, T., Sanjayan, J. G., and Cheng, Y.-B. (2002). Sulfate attack on alkali-activated slag concrete. *Cem. Concr. Res.* 32 (2), 211–216. doi:10.1016/s0008-8846(01)00659-7

Bondar, D., Ma, Q., Soutsos, M., Basheer, M., Provis, J. L., and Nanukuttan, S. (2018). Alkali activated slag concretes designed for a desired slump, strength and chloride diffusivity. *Constr. Build. Mater.* 190, 191–199. doi:10.1016/j.conbuildmat.2018.09.124

Chi, M. (2012). Effects of dosage of alkali-activated solution and curing conditions on the properties and durability of alkali-activated slag concrete. *Constr. Build. Mater.* 35, 240–245. doi:10.1016/j.conbuildmat.2012.04.005

Collins, F., and Sanjayan, J. G. (2000). Cracking tendency of alkali-activated slag concrete subjected to restrained shrinkage. *Cem. Concr. Res.* 30 (5), 791–798. doi:10.1016/s0008-8846(00)00243-x

Dai, X., Aydin, S., Yardimci, M. Y., and De Schutter, G. (2022). Early structural build-up, setting behavior, reaction kinetics and microstructure of sodium silicate-activated slag mixtures with different retarder chemicals. *Cem. Concr. Res.* 159, 106872. doi:10.1016/j.cemconres.2022.106872

Díaz, Y. C., Berriel, S. S., Heierli, U., Favier, A. R., Machado, I. R. S., Scrivener, K. L., et al. (2017). Limestone calcined clay cement as a low-carbon solution to meet expanding cement demand in emerging economies. *Dev. Eng.* 2, 82–91. doi:10.1016/j.deveng.2017.06.001

Fu, Q., Bu, M., Zhang, Z., Xu, W., Yuan, Q., and Niu, D. (2023). Hydration characteristics and microstructure of alkali-activated slag concrete: a review. *Engineering* 20, 162–179. doi:10.1016/j.eng.2021.07.026

Geng, Z., Tang, S., Wang, Y., A, H., He, Z., Wu, K., et al. (2024). Stress relaxation properties of calcium silicate hydrate: a molecular dynamics study. *J. Zhejiang University-SCIENCE A* 25 (2), 97–115. doi:10.1631/jzus.a2300476

Huang, J., Zou, C., Sun, D., Yang, B., and Yan, J. (2021). Effect of recycled fine aggregates on alkali-activated slag concrete properties. *Structures* 30, 89–99. doi:10.1016/j.istruc.2020.12.064

Huo, Y., Hu, S., Lu, D., Han, X., Sun, H., Ma, X., et al. (2023b). Understanding the roles of Li2CO3 in a sulphoaluminate cement system at negative temperatures. *Case Stud. Constr. Mater.* 19, e02574. doi:10.1016/j.cscm.2023.e02574

Huo, Y., Huang, J., Han, X., Sun, H., Liu, T., Zhou, J., et al. (2023d). Mass GGBFS concrete mixed with recycled aggregates as alkali-active substances: workability, temperature history and strength. *Materials* 16 (16), 5632. doi:10.3390/ma16165632

Huo, Y., Huang, J., Lu, D., Han, X., Sun, H., Liu, T., et al. (2023c). Durability of alkali-activated slag concrete incorporating silica fume and rice husk ash. *J. Build. Eng.* 78, 107637. doi:10.1016/j.jobe.2023.107637

Huo, Y., Huang, J., Xu, N., Lu, D., Han, X., Sun, H., et al. (2024). Comparison of stearic acid and oleic acid for shrinkage-mitigating of alkali-activated slag composites. *J. Sustain. Cement-Based Mater.* 13, 436–449. doi:10.1080/21650373.2023.2280915

Huo, Y., Liu, T., Lu, D., Han, X., Sun, H., Huang, J., et al. (2023f). Dynamic tensile properties of steel fiber reinforced polyethylene fiber-engineered/strain-hardening cementitious composites (PE-ECC/SHCC) at high strain rate. *Cem. Concr. Compos.* 143, 105234. doi:10.1016/j.cemconcomp.2023.105234

Huo, Y., Lu, D., Han, X., Hu, S., Sun, H., Zhang, C., et al. (2023a). The role of admixed CaO in a sulphoaluminate cement system under winter environments. *J. Build. Eng.* 78, 107638. doi:10.1016/j.jobe.2023.107638

Huo, Y., Lu, D., Wang, Z., Liu, Y., Chen, Z., and Yang, Y. (2023e). Bending behavior of strain hardening cementitious composites based on the combined fiber-interface constitutive model. *Comput. Struct.* 281, 107017. doi:10.1016/j.compstruc.2023.107017

Huo, Y., Sun, H., Chen, Z., and Yang, Y. (2022a). Mechanical properties and its reliability prediction of engineered/strain-hardening cementitious composites (ECC/SHCC) with different moisture contents at negative temperatures. *Cem. Concr. Compos.* 134, 104812. doi:10.1016/j.cemconcomp.2022.104812

Huo, Y., Sun, H., Lu, D., Chen, Z., and Yang, Y. (2022b). Mechanical properties of concrete at low and ultra-low temperatures-a review. *J. Infrastructure Preserv. Resil.* 3 (1), 20. doi:10.1186/s43065-022-00063-4

Juenger, M., Winnefeld, F., Provis, J. L., and Ideker, J. (2011). Advances in alternative cementitious binders. *Cem. Concr. Res.* 41 (12), 1232–1243. doi:10.1016/j.cemconres.2010.11.012

Karikatti, V., Chitawadagi, M. V., Devarangadi, M., Sanjith, J., and Gangadhara Reddy, N. (2023). Influence of bagasse ash powder and marble powder on strength and microstructure characteristics of alkali activated slag concrete cured at room temperature for rigid pavement application. *Clean. Mater.* 9, 100200. doi:10.1016/j.clema.2023.100200

Liao, Y., Wang, S., Wang, K., Qunaynah, S. A., Wan, S., Yuan, Z., et al. (2023b). A study on the hydration of calcium aluminate cement pastes containing silica fume using non-contact electrical resistivity measurement. *J. Mater. Res. Technol.* 24, 8135–8149. doi:10.1016/j.jmrt.2023.05.080

Liao, Y., Yao, J., Deng, F., Li, H., Wang, K., and Tang, S. (2023a). Hydration behavior and strength development of supersulfated cement prepared by calcined phosphogypsum and slaked lime. *J. Build. Eng.* 80, 108075. doi:10.1016/j.jobe.2023.108075

Lu, D., Fu, C., Jiang, X., Chen, Z., Qu, F., Huo, Y., et al. (2024c). Sustainable microwave-heating healing asphalt concrete incorporating functional aggregates and waste ferrite. *Transp. Res. Part D Transp. Environ.* 129, 104117. doi:10.1016/j.trd.2024.104117

Lu, D., Huo, Y., Jiang, Z., and Zhong, J. (2023b). Carbon nanotube polymer nanocomposites coated aggregate enabled highly conductive concrete for structural health monitoring. *Carbon* 206, 340–350. doi:10.1016/j.carbon.2023.02.043

Lu, D., Jiang, X., and Leng, Z. (2024a). Sustainable microwave-heating healing asphalt concrete fabricated with waste microwave-sensitive fillers. *J. Clean. Prod.* 434, 140343. doi:10.1016/j.jclepro.2023.140343

Lu, D., Jiang, X., Leng, Z., Zhang, S., Wang, D., and Zhong, J. (2023a). Dual responsive microwave heating-healing system in asphalt concrete incorporating coal gangue and functional aggregate. *J. Clean. Prod.* 422, 138648. doi:10.1016/j.jclepro.2023.138648

Lu, D., Jiang, X., Qu, F., and Huo, Y. (2024b). Mitigating sulfate ions migration in concrete: a targeted approach to address recycled concrete aggregate's impact. *J. Clean. Prod.* 442, 141135. doi:10.1016/j.jclepro.2024.141135

Lu, D., Leng, Z., Lu, G., Wang, D., and Huo, Y. (2023c). A critical review of carbon materials engineered electrically conductive cement concrete and its potential applications. *Int. J. Smart Nano Mater.* 14 (2), 189–215. doi:10.1080/19475411.2023.2199703

Meyer, C. (2009). The greening of the concrete industry. *Cem. Concr. Compos.* 31 (8), 601–605. doi:10.1016/j.cemconcomp.2008.12.010

Ou, Z., Feng, R., Li, F., Liu, G., and Li, N. (2022). Development of drying shrinkage model for alkali-activated slag concrete. *Constr. Build. Mater.* 323, 126556. doi:10.1016/j.conbuildmat.2022.126556

Purnell, P. (2013). The carbon footprint of reinforced concrete. *Adv. Cem. Res.* 25 (6), 362–368. doi:10.1680/adcr.13.00013

Sadeghian, G., Behfarnia, K., and Teymouri, M. (2022). Drying shrinkage of one-part alkali-activated slag concrete. *J. Build. Eng.* 51, 104263. doi:10.1016/j.jobe.2022.104263

Tang, S., Wang, Y., Geng, Z., Xu, X., Yu, W., A, H., et al. (2021). Structure, fractality, mechanics and durability of calcium silicate hydrates. *Fractal Fract.* 5, 47. doi:10.3390/fractalfract5020047

Thomas, R., Gebregziabiher, B. S., Giffin, A., and Peethamparan, S. (2018). Micromechanical properties of alkali-activated slag cement binders. *Cem. Concr. Compos.* 90, 241–256. doi:10.1016/j.cemconcomp.2018.04.003

Wang, L., Guo, F., Lin, Y., Yang, H., and Tang, S. W. (2020). Comparison between the effects of phosphorous slag and fly ash on the C-S-H structure, long-term hydration heat and volume deformation of cement-based materials. *Constr. Build. Mater.* 250, 118807. doi:10.1016/j.conbuildmat.2020.118807

Wang, L., Jin, M., Zhou, S., Tang, S., and Lu, X. (2021). Investigation of microstructure of C-S-H and micro-mechanics of cement pastes under NH4NO3 dissolution by 29Si MAS NMR and microhardness. *Measurement* 185, 110019. doi:10.1016/j.measurement.2021.110019

Weil, M., Dombrowski, K., and Buchwald, A. (2024). Life-cycle analysis of geopolymers. *Geopolymers, Elsevier2009*, 194–210. doi:10.1533/9781845696382.2.194

Yin, B., Li, G., Zhang, Y., and Liew, K. (2023). Sustainability-driven atomistic model for exploring the mechanical properties of low carbon limestone calcined clay cement (LC3). *J. Clean. Prod.* 412, 137394. doi:10.1016/j.jclepro.2023.137394

Zhang, J., Shi, C., Zhang, Z., and Ou, Z. (2017). Durability of alkali-activated materials in aggressive environments: a review on recent studies. *Constr. Build. Mater.* 152, 598–613. doi:10.1016/j.conbuildmat.2017.07.027

Zhao, K., Liang, Y., Ji, T., Lu, Y., and Lin, X. (2020). Effect of activator types and concentration of CO2 on the steel corrosion in the carbonated alkali-activated slag concrete. *Constr. Build. Mater.* 262, 120044. doi:10.1016/j.conbuildmat.2020.120044

Zheng, X., Lu, H., You, S., Cheng, K., Easa, S. M., Chen, Z., et al. (2022). Tensile creep behavior of Alkali-activated slag concrete incorporating lightweight aggregate. *Constr. Build. Mater.* 357, 129318. doi:10.1016/j.conbuildmat.2022.129318

Zhou, Y., Li, W., Peng, Y., Tang, S., Wang, L., Shi, Y., et al. (2023). Hydration and fractal analysis on low-heat portland cement pastes using thermodynamics-based methods. *Fractal Fract.* 7, 606. doi:10.3390/fractalfract7080606

Zhu, X., Kang, X., Deng, J., Yang, K., Jiang, S., and Yang, C. (2021). Chemical and physical effects of high-volume limestone powder on sodium silicate-activated slag cement (AASC). *Constr. Build. Mater.* 292, 123257. doi:10.1016/j.conbuildmat.2021.123257